Biophysical Chemistry 200–201 (2015) 34–40

Contents lists available at ScienceDirect

Biophysical Chemistry

journal homepage: http://www.elsevier.com/locate/biophyschem

Functional role of the conserved i-helix residue I346 in CYP5A1–Nanodiscs

Daryl D. Meling [a,1], Susan Zelasko [b,1], Amogh Kambalyal [b], Jahnabi Roy [d], Aditi Das [a,b,c,*]

[a] Department of Biochemistry, University of Illinois Urbana–Champaign, Urbana IL 61802, USA
[b] Department of Comparative Biosciences, University of Illinois Urbana–Champaign, Urbana IL 61802, USA
[c] Beckman Institute for Advanced Science and Department of Bioengineering, University of Illinois Urbana–Champaign, Urbana IL 61802, USA
[d] Department of Chemistry, University of Illinois Urbana-Champaign, IL 61802, USA

HIGHLIGHTS

- CYP5A1 has an Ile instead of the conserved, I-helix Thr found in most CYPs.
- Mutation of this Ile to a hydroxyl-containing residues Thr or Ser increases TXA_2 formation.
- Spectral changes are noted between the WT and hydroxyl-containing mutants.

GRAPHICAL ABSTRACT

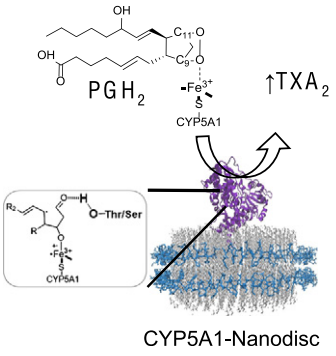

CYP5A1-Nanodisc

ARTICLE INFO

Article history:
Received 12 December 2014
Received in revised form 4 February 2015
Accepted 4 March 2015
Available online 12 March 2015

Keywords:
Eicosanoids
Cytochrome P450
Thromboxane synthase
Protein engineering
CYP5A1
Nanodiscs

ABSTRACT

Thromboxane synthase (CYP5A1) is a non-classical cytochrome P450 (CYP) expressed in human platelets that mediates vascular homeostasis by producing thromboxane A_2 (TXA_2) through the isomerization of prostaglandin H_2 (PGH_2). A homology alignment of CYP5A1 with human CYPs indicates that a highly conserved I-helix threonine residue is occupied by an isoleucine at position 346 in CYP5A1. We find that reverse-engineering CYP5A1 to contain either threonine or serine in this position dramatically increases TXA_2 formation. Interestingly, the levels of malondialdehyde (MDA), a homolytic fragmentation product of PGH_2 formed via a pathway independent of TXA_2 formation, remain constant. Furthermore, spectral analysis using two PGH_2 substrate analogs supports the observed activity changes in the hydroxyl-containing mutants. The more constrained active site of the I346T mutant displays altered PGH_2 substrate analog binding properties. Together these studies provide new mechanistic insights into CYP5A1 mediated isomerization of PGH_2 with respect to a critical active site residue.

1. Introduction

Cytochrome P450s (CYPs) are heme-containing enzymes that catalyze numerous oxidative reactions in nature including the hydroxylation and epoxidation of alkenes, as well as less commonly, the isomerization of endoperoxide-containing substrates [1]. In order to catalyze hydroxylation or epoxidation reactions, classical Type I and II

* Corresponding author at: Department of Comparative Biosciences, University of Illinois Urbana-Champaign, 3813 Veterinary Medicine Basic Sciences Building, 2001 South Lincoln Avenue, Urbana, IL 61802, USA. Tel.: +1 217 244 0630.
E-mail address: aditidas@illinois.edu (A. Das).
[1] Susan Zelasko and Daryl Meling have contributed equally to this paper.

http://dx.doi.org/10.1016/j.bpc.2015.03.002
0301-4622/

CYPs shuttle through heme–oxygen reactive intermediates such as iron–hydroperoxo and iron–oxenoid species (Supplementary Fig. S1). This hydroperoxo intermediate of the heme is thought to be stabilized by the hydroxyl group of a highly conserved threonine residue in the I-helix, positioned on the distal side of the heme active site (Supplementary Fig. S1 and S2) [2,3]. This residue mediates the formation of an appropriate hydrogen bonding network, either directly by the threonine group or by the positioning of a water molecule within the active site [3]. Previous mutagenesis studies on this threonine residue in other CYPs have shown that mutating this residue significantly impacts enzyme function. The alteration of this residue presumably destabilizes the iron–hydroperoxo intermediate, leading to a decrease in formation of the native hydroxylated or epoxygenated product and an increase in the production of reactive oxygen species [3–7]. The hydrogen bonding network facilitated by this threonine is also important in many CYPs for two proton transfer steps that allow the heme intermediate to transition from an iron–peroxo to an iron–hydroperoxo and then to an iron–oxenoid species, eventually leading to the epoxidation or hydroxylation of the substrate [8].

Interestingly, a sequence homology alignment of the known human CYPs show that there are a few human CYPs that lack this conserved threonine and instead contain isoleucine or asparagine (Supplementary Fig. S2 and S3). These CYPs are either isomerases (e.g. CYP5A1, CYP8A1) instead of typical hydroxylases or they have unknown functions (e.g. CYP20A1, CYP39A). Prostacyclin synthase (CYP8A1) has an asparagine (N287) residue instead of threonine and the CYP8A1 crystal structure suggests that the capacity to form a hydrogen-bond network through the asparagine remains [9]. In contrast, an isoleucine residue is present in two human CYPs, thromboxane synthase (CYP5A1) and the orphan CYP20A1, as well as in allene oxide synthase (CYP74A1) from the plant *Arabidopsis thaliana* [10,11]. Isoleucine is incapable of participating in a hydrogen bonding network and the purpose of this active site residue in product formation has not been thoroughly examined.

Of the two human CYPs with an isoleucine instead of a threonine, CYP5A1 has been studied more extensively and is known to mediate cardiovascular homeostasis by generating thromboxane A_2 (TXA_2). CYP5A1 is expressed in platelets [12] and converts prostaglandin H_2 (PGH_2) either into TXA_2 via an isomerization of the endoperoxide bond or into two fragmentation products, 12-L-hydroxy-5,8,10-heptadecatrienoic acid (HHT) and malondialdehyde (MDA) (Fig. 1) [13,14].

HHT is an endogenous ligand for the leukotriene B4 receptor BLT2 which is implicated in allergic airway inflammation [16]. The precise role of MDA remains undetermined, however, it has been found to form adducts with proteins, phospholipids [17], and DNA, particularly in atherosclerotic lesions [18]. Homeostatic imbalances in CYP5A1 that lead to the over-production of TXA_2 have been implicated in the development of several major disorders [19–22]. Owing to the unique biochemical nature and physiological significance of CYP5A1, it is important to better understand the mechanistic details of this enzyme with respect to this specific residue Ile346.

In this work, we have reverse-engineered the native isoleucine 346 to threonine in CYP5A1 in order to understand its role in substrate binding and product formation. We have also mutated this isoleucine 346 to serine, a smaller hydroxyl-containing residue, to examine the spatial constraints of the substrate orientation within the enzyme active site. Here we describe the biochemical characteristics of these mutants and show that the introduction of a hydroxyl-containing residue significantly influences native CYP5A1 function. All studies were performed using CYP5A1 in Nanodiscs (i.e. nanoscale lipid bilayers) that stabilize the enzyme in a native membrane environment. This produces reproducible and cleaner spectroscopic data and provides a native-like membrane environment to evaluate the enzyme function [23–30]. Hence, this work provides insights into the role of the key active site residue 346 in thromboxane synthase function within a native membrane environment with respect to substrate isomerization and substrate analog binding.

2. Results

2.1. Expression of CYP5A1 mutants and incorporation into Nanodiscs

We mutated the isoleucine at position 346 of CYP5A1 to threonine to investigate how a hydroxyl-containing residue near the catalytic heme would affect the native CYP5A1 reactions. In order to examine the potential influence of residue size on the binding and stabilization of the substrate within the enzyme active site, this position was also mutated to serine. The mutations were carried out using site-directed mutagenesis. The proteins were purified and incorporated into Nanodiscs as described in the Materials and Methods section. Protein purification yields are listed in Supplementary Table S1.

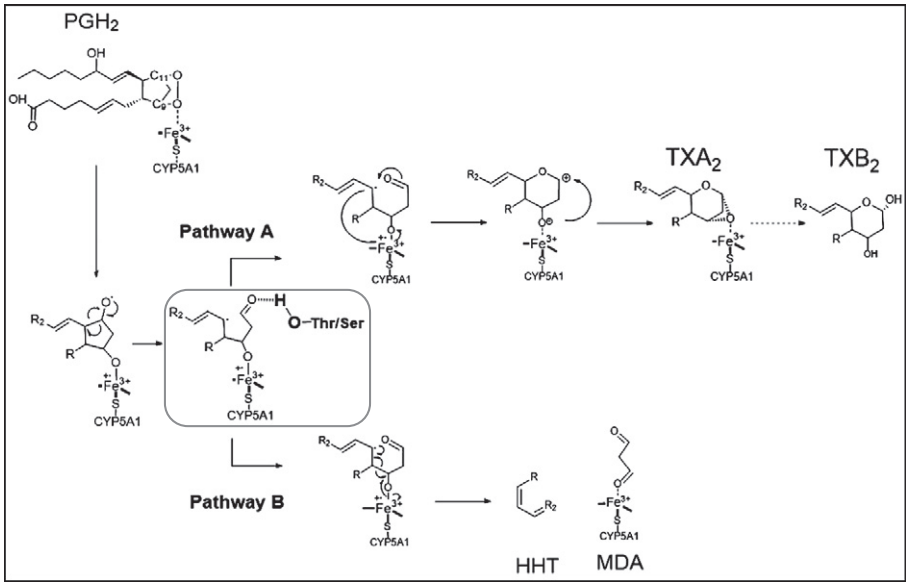

Fig. 1. Mechanism of TXA_2, MDA and HHT formation by CYP5A1. The proposed mechanism of TXA_2 formation followed by non-enzymatic hydrolysis to form TXB_2 is shown to follow pathway A [15]. Two fragmentation products (MDA and HHT) form via pathway B [15]. The boxed intermediate that precedes TXA_2 formation is likely better stabilized or repositioned in the active sites of the I346T and I346S CYP5A1 mutants.

2.2. Metabolism of PGH_2 by CYP5A1

CYP5A1 converts PGH_2 into the major physiological metabolite TXA_2, as well as MDA and HHT. TXA_2 rapidly hydrolyzes non-enzymatically to TXB_2 (Fig. 1). The enzymatic activity of CYP5A1 and the mutants was determined by quantifying the TXB_2 and MDA formation following incubation of CYP5A1–Nanodiscs (CYP5A1–ND) with PGH_2. The amount of TXB_2 formed via Pathway A was determined using an ELISA-based detection method and MDA was monitored spectroscopically at 268 nm (Fig. 2). Mechanistically, MDA and HHT are formed in an equimolar ratio, hence, only MDA was monitored to track pathway B (Fig. 1). Quantification of MDA and TXB_2 revealed that the mutation from isoleucine to a hydroxyl-containing threonine or serine residue caused an approximately two-fold increase in TXB_2 production. The I346T mutant produced 239% and the I346S mutant produced 161% TXB_2, relative to wild-type. Interestingly, MDA and HHT formation, which was at a higher overall rate than TXB_2 production, remained statistically constant for wild-type and I346 mutants of CYP5A1–ND. Lipids in the Nanodiscs were 100% POPC, which allow statistically the same amount of TXB_2 production as a more physiological lipid mixture of POPC/POPE/POPS (53:40:7) [30]. Additionally, the product ratio of the mutants was unaffected by the use of Nanodiscs (data not shown) and the Nanodisc system yielded reproducible data.

2.3. Spectral characterization

The oxidized spectra of the CYP5A1–ND wild-type, I346T, and I346S proteins had Soret peaks at 417 nm, 417 nm, and 419 nm, respectively, with the α and β bands (Q-bands) appearing near 536 nm and 570 nm, respectively. Determination of the heme content and assessment of protein folding was obtained from a dithionite-reduced CO bound spectrum of the heme proteins (Table 1). The Fe(II) CO-bound complex formed showed a 452 nm and 451 nm peak in the wild-type and I346T mutant proteins, respectively. The I346S mutant showed a red-shifted CO-bound spectrum at 454 nm, indicating that the active site had become more polar or that the hydroxyl of the serine residue may interact with the heme group [31,32] (Supplementary Fig. S5).

Table 1
Spectral characterization of CYP5A1–ND and mutants. The average wavelength shift (λ) and dissociation constant values (K_d) with standard deviations were obtained from spectral titrations, performed in duplicate.

Spectral characteristics of CYP5A1–ND			
	WT	I346T	I346S
Oxidized (nm)	417	417	419
Reduced (nm)	412	412	413
CO-bound (nm)	452	451	454
Aver. λ shift for U46619 (nm)	3.0 ± 0.0*	4.0 ± 0.0	8.5 ± 0.7
Aver. λ shift for U44069 (nm)	4.0 ± 0.0*	4.5 ± 0.7	5.5 ± 0.7
U44069 K_d (μM)	6 ± 3.0*	5.0 ± 0.3	4.0 ± 1.8
U46619 K_d (μM)	5 ± 4.0*	15 ± 3.0	2.9 ± 0.1

* Previously published data [30].

2.4. Equilibrium binding studies of CYP5A1 with substrate analogs

We further performed spectral titrations using two analogs of the native substrate PGH_2, U44069 and U46619. The analog 9,11-epoxymethano PGH_2 (U44069) has an oxygen atom at the C9 position, while the analog 11,9-epoxymethano PGH_2 (U46619) has an oxygen atom at the C11 position. In both cases, an oxygen of the endoperoxide bond is replaced by a methylene group making a CH_2–O bond instead of an O–O bond (Figs. 1 and 3).

There were some interesting differences in the binding of the substrate analogs to the I346T and I346S mutants. The binding of U44069 to wild-type CYP5A1–ND that is thought to reflect native PGH_2 binding showed a typical trough near 426 nm and a peak near 409 nm, as expected [30]. The spectral dissociation constant (K_d) for binding of U44069 to wild-type CYP5A1–ND is 6.0 ± 3.0 μM, to the I346T mutant is 5.0 ± 0.3 μM, and to the I346S mutant is 4.0 ± 1.8 μM. The UV–vis spectral wavelength shifts due to U44069 binding were nearly constant for all mutants (Table 1). While spectral perturbations seen with respect

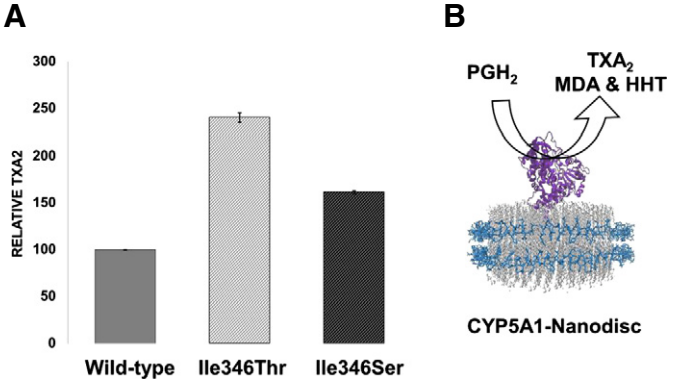

Average Product Formation		
	Relative Production of MDA compared to WT	Relative Production of TXB_2 compared to WT
Wild-Type	100 ± 1.7%	100 ± 0.27%
Ile346Thr	107 ± 20.2%	239 ± 4.9%
Ile346Ser	96 ± 4.2%	161 ± 1.6%

Fig. 2. Relative product formation of CYP5A1 mutants. Addition of the native substrate PGH_2 to CYP5A1 in Nanodiscs results in the formation of TXA_2, MDA and HHT. MDA was measured using UV–visible spectroscopy, while TXB_2 (the hydrolysis product of TXA_2), was measured using a standard ELISA kit. (Top) (A) Results for assays with CYP5A1–ND WT, I346T, and I346S performed are reported along with standard error. (B) Schematic showing the conversion of PGH_2 into TXA_2, MDA and HHT by CYP5A1–ND. The protein CYP5A1 (purple) is incorporated into the lipid bilayers (white) and these layers are surrounded by membrane scaffold protein (blue). (Bottom) Table showing the average product formation from Panel A with standard deviations.

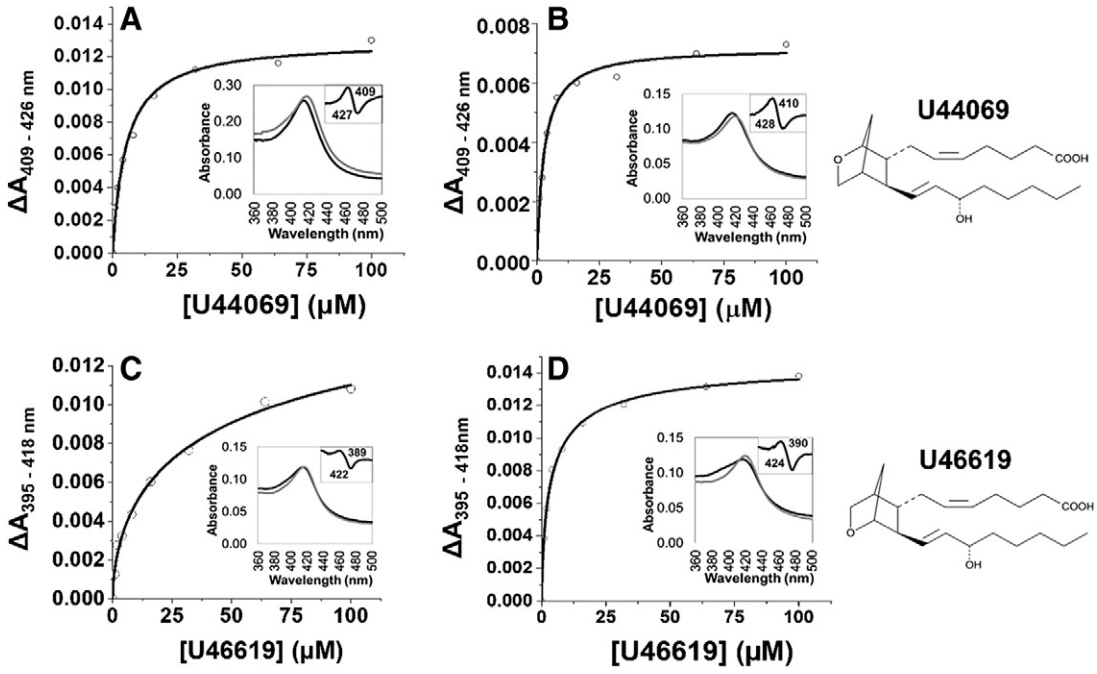

Fig. 3. Equilibrium binding studies of CYP5A1–ND with substrate analogs. The binding of substrate analog U44069 to (A) CYP5A1–ND I346T and (B) CYP5A1–ND I346S showed an average K_d of binding of 5.0 ± 0.3 μM and 4.0 ± 1.8 μM for I346T and I346S, respectively. The binding of substrate analog U46619 to (C) CYP5A1–ND I346T and (D) CYP5A1–ND I346S showed an average K_d of binding of 15 ± 3.0 μM and 2.9 ± 0.1 μM for I346T, and I346S, respectively. (Insets) Absorbance spectra of equilibrium binding of CYP5A1–ND with substrate analogs.

to binding U44069 were not significant, those observed for the binding of U46619 with the mutants were significant.

The difference spectrum of each CYP5A1–ND bound to U46619 shows a characteristic high-spin state based on a peak shift to around 390 nm, which suggests that the C9 methylene group of the analog is near the CYP-bound heme. Interestingly, the I346S mutant of U46619-bound CYP5A1–ND produced red-shifted UV–vis spectral shifts of 8.5 ± 0.7 nm compared to 4 ± 0.0 nm and 3 ± 0.0 nm for the I346T mutant and wild-type CYP5A1–ND, respectively (Table 1; Fig. 3) [30]. There is significant decrease in the binding affinity with U46619 and the I346T mutant (K_d is 15 ± 3 μM) (Table 1) compared to the I346S mutant. It is likely that the smaller cavity near the active site in the I346T versus the I346S mutant appears to accommodate U46619 to a lesser extent, leading to lower binding affinity in the I346T mutant.

2.5. LC–MS analysis of product formation by mutant CYP5A1

We determined the product profiles of the wild-type and the threonine and serine mutants of CYP5A1 following incubation with PGH_2 using LC–MS as described in the Materials and Methods section. No novel products were detected in the mutant proteins beyond those quantified using UV–vis spectroscopy and ELISA.

3. Discussion

3.1. The role of the isoleucine residue in CYP5A1

The vast majority of CYPs contain a highly conserved threonine residue positioned on the distal side of the heme active site; however, the role of this residue is variable [2,3]. In many classical CYPs, the threonine hydroxyl group is believed to be involved in hydrogen-binding and proton delivery to the heme-bound oxygen during reactions [5,33]. In CYP8A1, the conserved I-helix threonine is replaced with an asparagine residue that is capable of forming hydrogen-binding networks through the available nitrogens [9]. In contrast, CYP5A1 contains an isoleucine in place of this conserved threonine [12,14]. It is important to note that the close placement of this residue on the distal side of the heme active site can significantly influence native catalytic function. Therefore, the introduction of a hydroxyl near the heme may change the capacity of CYP5A1 towards radical stabilization. In the absence of a crystal structure for CYP5A1, we prepared a Molecular Operating Environment (MOE) model of CYP5A1 bound to PGH_2 that indicated that both isoleucine and the hydroxyl groups of threonine and serine are within 4 to 6 Å of the heme active site (Fig. 4 and Supplementary Fig. S6).

Mutation of isoleucine 346 to hydroxyl-containing residues increased native product formation of TXA_2, confirming the influence of this residue position on CYP5A1 catalysis [34]. Excess TXA_2 is detrimental to cardiovascular health, thus this naturally occurring I346 residue may deviate from the conserved hydrogen-bonding residues in order to attenuate TXA_2 levels *in vivo*.

3.2. Mechanistic interpretation of the increase of thromboxane formation in I346T and I346S mutants

From a mechanistic standpoint, the isomerization of PGH_2 by CYP5A1 has been proposed to follow the Fe(III)–porphyrin pi–cation radical route that involves a bifurcation of a key intermediate into two different pathways leading to separate products [15] (Fig. 1). In pathway A, PGH_2 is converted to TXA_2 and in pathway B, PGH_2 is fragmented to MDA and HHT (Fig. 1). The PGH_2 endoperoxide consists of two oxygens attached to carbons at positions C11 and C9. The oxygen attached at the C9 position interacts with heme at the active site (Fig. 1) while the oxygen attached at the C11 position forms the carbonyl group in the intermediates preceding product formation. We hypothesize that this oxygen attached at the C11 position is stabilized by hydrogen bonding in the I346T and I346S mutants. This stabilization would favor the cyclization of the intermediate leading to TXA_2 formation, but has no effect on the fragmentation of this intermediate to form MDA and HHT. Evidence to support this hypothesis stems from the observation that upon binding U46619, in which the oxygen attached to the C11 carbon is proposed to be near the hydroxyl of the threonine or serine residue in the mutated protein, the Soret peak shifts by as much as 8.5 ± 0.7 nm

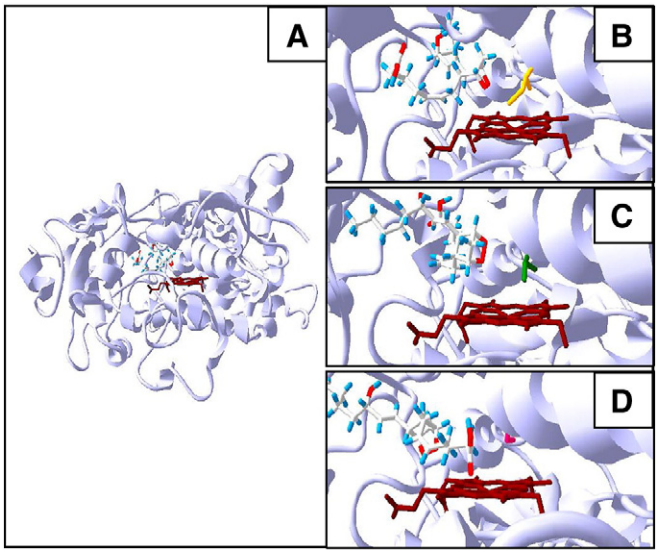

Fig. 4. Energy Minimized MOE active site models. Full view of (A) CYP5A1 WT bound to PGH_2 with the active site heme shown in red. Panels (B–D) show the PGH_2-bound CYP5A1 active sites of the following: (B) Wild type with isoleucine in yellow, (C) I346T mutant with threonine in green, and (D) I346S mutant with serine in magenta. The protein is represented as blue ribbons. The endoperoxide oxygens bound at carbon positions C9 and C11 are displayed in red near the heme. Note, however, that the binding of PGH_2 into the serine active site is different from the wild-type and I346T proteins, placing the oxygens at carbon positions C9 and C11 further away from the heme.

for the I346S mutant. Interestingly, no such spectral shifts were observed using the U44069 where a $–CH_2–$ group replaces the C11 oxygen in U46619 [30]. Additionally, the increased polarity of the mutant active sites due to the presence of a hydroxyl group may in general facilitate the electron transfer from the PGH_2 intermediate to the heme moiety as a part of TXA_2 formation. However, this does not explain the observed spectral changes discussed above.

3.3. I346S vs. I346T, the role of the smaller residue

We observed that the I346S mutant shows an 8.5 ± 0.7 nm wavelength shift on binding U46619 (Table 1; Fig. 3). Moreover, the Fe(II)–CO-bound spectrum is more red-shifted for the I346S mutant suggesting a change in the electronic environment of the heme due to the orientation of the polar serine group [31,32]. When threonine is changed to serine at this position in other CYPs, there is a precedent for a wider range of products being formed. For instance, a change in substrate orientation and specificity was observed when the conserved T303 of CYP2E1 was mutated to serine, along with a change from high-spin to mixed-spin in the ferric absorption spectrum [35]. This is presumably due to the greater freedom of movement of the substrate. In our studies we did not detect any additional products using LC–MS, however, the I346S mutant did display altered activity and more extreme spectral characteristics from those of the wild-type and I346T mutant.

4. Conclusions

In summary, in this paper we uncover new aspects of CYP5A1 function. Firstly, we reverse-engineered the native isoleucine in CYP5A1 I-helix to the conserved threonine found in classical CYPs to understand the role of this residue in product formation by CYP5A1. Upon mutation of I346 to threonine we observed a 239% increase in thromboxane formation while MDA and HHT formation remained almost the same. Excess thromboxane is detrimental to cardiovascular health, thus this naturally occurring I346 residue might help in keeping the levels of thromboxane lower in the platelets in the human body. In addition, we mutated this I-helix residue to serine, a smaller hydroxyl-containing residue, in order to gain a better understanding of the spatial constraints of the active site, polarity of this residue, and substrate orientation. Again, we saw an increase in the production of thromboxane without any concomitant increase in MDA or HHT. Based on spectral characterizations, we hypothesized that the selective increase in the production of thromboxane is due to stabilization of the C11 oxygen of the carbonyl in the intermediate by hydrogen-bonding interactions between the hydroxyl moiety of threonine and with the oxygen atom at C11 of the substrate PGH_2. The hydroxyl-containing residue selectively stabilizes the reaction pathway leading to TXA_2 formation, but would not alter the MDA and HHT fragmentation pathway. Evidence to support this hypothesis comes from the observation that the binding of U46619, which only has an oxygen bound at the C11 position, to the threonine or serine mutants significantly perturbs their Sorets.

5. Materials and methods

5.1. Materials

The human CYP5A1 gene was obtained from Origene. PCR reagents were purchased from New England Biolabs. Molecular biology enzymes and *Escherichia coli* DH5α were purchased from Invitrogen. Plasmid DNA was purified using a Qiagen Gel Extraction kit. Ampicillin (Amp), arabinose, chloramphenicol (Chlr), isopropyl β-D-1-thiogalactopyranoside (IPTG), and Ni-NTA resin were bought from Gold Biotechnology. δ-Aminolevulinic acid (δ-ALA) was purchased from Frontier Scientific. 1-palmitoyl-2-oleoyl-sn-glycero-3-phosphocholine (POPC) was purchased from Avanti Polar Lipids. PGH_2, 9,11-dideoxy-9α,11α-epoxymethano Prostaglandin F2α (U44069), and 9,11-dideoxy-9α,11α-methanoepoxy Prostaglandin F2α (U46619) were purchased from Cayman Chemicals. NADPH was purchased from P212121.com. The TXB_2 ELISA kit was purchased from Oxford Biomedical Research.

5.2. Protein engineering of CYP5A1

The CYP5A1 gene (Origene) was cloned into the pAr5 (modified pCWOri+) plasmid using the NdeI and XbaI restriction fragment sites located downstream of the IPTG-inducible tac promoter with Amp resistance. The CYP5A1 protein was modified by truncating the first 29 amino acids, incorporating an N-terminal hydrophilic sequence MAKKTSS, and a C-terminal 6-histidine tag [30]. The plasmids were amplified and purified using a Qiagen Plasmid mini-prep kit (Valencia, CA). The I346T and I346S mutations were made using forward primers containing single nucleotide substitutions at residue 346. The reverse primer was phosphorylated with T4 polynucleotide kinase (New England Biolabs). The forward and reverse primer sequences are listed in Supplementary Fig. S4. The PCR reaction consisted of 1 μM of forward and reverse primers in HF reaction buffer (New England Biolabs) containing 50 pg/μL CYP5A1-containg plasmid, 200 μM dNTPs, 5% DMSO, and Phusion DNA polymerase (10 U/mL). The PCR thermocycler was set to 95 °C for 3 min, 20 cycles (95 °C for 30 s, 65 °C for 30 s), and then 72 °C for 4 min. Chemically competent DH5α cells were transformed by heat shock at 42 °C for 45 s, then set on ice. The addition of 1 mL of warm Super Optimal Broth (SOC) media was followed by shaking (250 rpm) at 37 °C for 1 h. Cells were plated on LBAmp in order to screen for the desired mutant plasmid. The mutant dsDNA was confirmed by DNA sequencing.

5.3. Expression of CYP5A1 mutants

The expression of the CYP5A1 mutants was performed as previously described [30,36,37].

5.4. Carbon monoxide binding assay

The heme content of the purified CYP5A1 protein was analyzed using UV–vis spectroscopy (Agilent Technologies, Santa, Clara CA) as previously described [30].

5.5. PGH_2 assay and TXB_2 quantification

The enzymatic activity of each protein was determined by quantifying TXB_2 and MDA formation using a Cary 300 UV–vis spectrometer (Agilent Technologies) in scan mode and a competitive binding ELISA assay read using a microplate reader at 650 nm, respectively, as described previously [30,38].

5.6. Equilibrium binding of CYP5A1–ND with substrate analog

The binding of substrate analogs U44069 and U46619 to CYP5A1–ND mutants were performed by spectroscopic titrations with each analog. First, each CYP5A1–ND mutant (WT, I346T, and I346S) at final concentrations of 0.5 μM in potassium phosphate buffer was incubated with increasing concentrations of U44069 or U46619, ranging from final concentrations of 0 to 100 μM dissolved in ethanol such that the final ethanol concentration did not exceed 1.5%. The absorbance readings were measured using a Cary 300 UV–vis spectrometer (Agilent Technologies) in full scan mode. The data was analyzed using MATLAB by taking a difference spectrum of the absorbance peaks and troughs at wavelengths of 426 and 409 nm for U44069 and 418 and 395 nm for U46619, then plotting absorbance change versus analog concentration in Origin Lab (Origin Lab, Northampton, MA). The data was fit using the Hill equation (Eq. (1)).

$$\Delta A = \frac{A_{\max} \cdot S^n}{K_s^n + S^n}, \tag{1}$$

In Eq. (1), ΔA is the absorbance difference at 426 and 409 nm for U44069 and 418 and 395 nm for U46619, A_{max} is the amplitude corresponding to maximal spin shift, K_s is the spectral dissociation constant, S is the substrate concentration, and n is the Hill coefficient. The binding data fit closely to $n = 1$. Therefore, for final fitting a single binding isotherm was used. The calculated spectral binding constants are averages of two independent experiments.

5.7. Assembly of CYP5A1–Nanodiscs

CYP5A1–ND were assembled as previously described [30,36,37] from a mixture of CYP5A1, membrane scaffold protein (MSPD1(−)), cholate, and POPC lipids by removing the detergents using Amberlite® [39,40] and cleaving the histidine tag of MSP1D1 [41].

5.8. Liquid chromatography–mass spectrophotometric analysis

PGH_2 (20 μM) was added to CYP5A1 suspended in Tris–Cl buffer (200 nM, pH 8.0). MDA formation was monitored spectroscopically at 268 nm for 3 min. This reaction was quenched with one volume of ethyl acetate and the organic layer was removed and re-extracted with another volume of ethyl acetate. The organic layers were dried under N_2 gas and resuspended in ethanol. The products were monitored by an LC–MS system that consisted of a Waters Alliance 2795 analytical high-performance-liquid-chromatography separation module (Waters, Milford, MA) coupled to an electrospray ionization mass spectrometer (Waters Quattro Ultima, Waters, Milford, MA) operated in negative ion mode. The sample was analyzed using a reverse-phase C18, 1.3 Å, 2.1 mm × 20 mm and 2.5 μm pore size column (Waters, Milford, MA) at a flow rate of 0.2 mL/min. The solvent system was composed of two solutions: solvent A (95% H_2O, 5% acetonitrile and 0.1% formic acid (FA)) and solvent B (5% H_2O and 95% ACN, and 0.1% FA). The 40 min gradient LC separation consisted of a linear gradient 35% → 85% solvent B.

5.9. Molecular Operating Environment Modeling and Ligand Docking

The models of CYP5A1 WT, I346T, and I346S were developed using homology modeling in PHYRE2 [42]. An open conformation of the CYP5A1 model was generated and used for subsequent ligand binding studies in Molecular Operating Environment software (MOE) (Chemical Computing Group Inc., Montreal, QC, Canada). Docking was performed using the Dock module of MOE. The activity site cavity was identified near the heme in the homology model of each protein. The ligand PGH_2 was prepared in the MOE Molecular Editor module and was docked into the cavities to generate possible ligand conformations. The default nonstochastic Triangle Matcher placement method was used as well as molecular mechanics refinement. Ten models with the ligand bound within the cavity with the endoperoxide oxygens near the heme (less than 7 Å) were generated and chosen for energy minimization. The models were verified by review of the Ramachandran torsion angles of amino acid residues. The energy minimized CYP5A1 models with the substrate docked were used to measure the average distances from the heme iron to the hydroxyl group of the mutated 346 residue and to the endoperoxide oxygens of the substrate. Interaction energies, which indicate the change of free energy when the substrate is bound, were compared for all three mutants.

Author contributions

All authors have given approval to the final version of the manuscript. D.D.M. and A.D. designed research; S.Z., and D.D.M. performed research; S.Z. and D.D.M. analyzed data; A.D. and S.Z. wrote the paper. A.K assisted in MOE modeling of CYP5A1. J.R. edited the paper and did some activity assay.

Abbreviations

CYP74A1	*Arabidopsis thaliana* allene oxide synthase
CYP2E1	cytochrome P450 2E1
CYP2J2	cytochrome P450 2 J2
CYP5A1	human thromboxane synthase
CYP5A1–ND	CYP5A1–Nanodiscs
CYP8A1	human prostacyclin synthase
HHT	12-L-hydroxy-5,8,10-heptadecatrienoic acid
MDA	malondialdehyde
MOE	Molecular Operating Environment
MSP	membrane scaffold protein
ND	Nanodisc
CYP	cytochrome P450
PGH_2	prostaglandin H_2
POPC	1-Palmitoyl-2-Oleoyl-sn-Glycero-3-Phosphocholine
SOC	Super Optimal Broth with glucose
TBXAS1	thromboxane synthase gene
TXA_2	thromboxane A_2
TXB_2	thromboxane B_2
U44069	9,11-dideoxy-9α,11α-epoxymethano Prostaglandin F2α
U46619	9,11-dideoxy-9α,11α-methanoepoxy Prostaglandin F2α

Acknowledgments

We thank Mr. Daniel McDougle for his help with data analysis. We thank Prof. Stephen Sligar for providing the gene encoding MSP1D1, membrane scaffold protein. We thank Prof. Ferguson, Prof. Ko, and Prof. Bagchi for generously sharing their laboratory equipment. We thank Prof. Mary Schuler, Mr. Brendon Colón, and Mr. Eryk Radziszewski for their training and assistance with the MOE modeling software. This project was supported by funding from the University

of Illinois Urbana–Champaign start-up funds, Research Board grant, and the American Heart Association.

Appendix A. Supplementary data

Supplementary data to this article can be found online at http://dx.doi.org/10.1016/j.bpc.2015.03.002.

References

[1] M. Waterman, I. Pikuleva, Cytochrome P450, Encyclopedia of Molecular Cell Biology and, Molecular Medicine, 2006.
[2] S.E. Graham-Lorence, J.A. Peterson, Structural alignments of P450s and extrapolations to the unknown, Methods Enzymol. 272 (1996) 315–325.
[3] H. Yeom, S. Sligar, H. Li, T. Poulos, A. Fulco, The role of Thr268 in oxygen activation of cytochrome P450BM-3, Biochemistry 34 (1995) 14733–14740.
[4] Y. Imai, M. Nakamura, Point Mutations at threonine-301 modify substrate specificity of rabbit liver microsomal cytochromes P450 (Laurate (ω-1) hydroxylase and testosterone 16α- hydroxylase), Biochem. Biophys. Res. Commun. 158 (1989) 717–722.
[5] J. Clark, C. Miles, C. Mowat, M. Walkinshaw, G. Reid, S. Daff, S. Chapman, The role of Thr268 and Phe393 in cytochrome P450 BM3, J. Inorg. Biochem. 100 (2006) 1075–1090.
[6] H. Furuya, T. Shimizu, K. Hirano, M. Hatano, Y. Fujii-Kuriyama, R. Raag, T. Poulos, Site-Directed Mutageneses of Rat Liver Cytochrome P-450$_d$: Catalytic Activities toward Benzphetamine and 7-Ethoxycoumarin, Biochemistry 28 (1989) 6848–6857.
[7] Y. Nitahara, K. Kishimoto, Y. Yabusaki, O. Gotoh, Y. Yoshida, T. Horiuchi, Y. Aoyama, The amino acid residues affecting the activity and azole susceptibility of rat CYP51 (Sterol 14-demethylase P450), J. Biochem. 129 (2001) 761–768.
[8] A.D. Vaz, D.F. McGinnity, M.J. Coon, Epoxidation of olefins by cytochrome P450: evidence from site-specific mutagenesis for hydroperoxo–iron as an electrophilic oxidant, Proc. Natl. Acad. Sci. U. S. A. 95 (1998) 3555–3560.
[9] C.W. Chiang, H.C. Yeh, L.H. Wang, N.L. Chan, Crystal structure of the human prostacyclin synthase, J. Mol. Biol. 364 (2006) 266–274.
[10] A.R. Brash, Mechanistic aspects of CYP74 allene oxide synthases and related cytochrome P450 enzymes, Phytochemistry 70 (2009) 1522–1531.
[11] D.R. Nelson, T. Kamataki, D.J. Waxman, F.P. Guengerich, R.W. Estabrook, R. Feyereisen, F.J. Gonzalez, M.J. Coon, I.C. Gunsalus, O. Gotoh, The P450 superfamily: update on new sequences, gene mapping, accession numbers, early trivial names of enzymes, and nomenclature, DNA Cell Biol. 12 (1993) 1–51.
[12] V. Ullrich, R. Nusing, Thromboxane synthase: from isolation to function, Stroke 21 (1990) 134–138.
[13] L.-H. Wang, A.-L. Tsai, P.-Y. Hsu, Substrate binding is the rate-limiting step in thromboxane synthase catalysis, J. Biol. Chem. 276 (2001) 14737–14743.
[14] M. Hecker, V. Ullrich, On the mechanism of prostacyclin and thromboxane A2 biosynthesis, J. Biol. Chem. 264 (1989) 141–150.
[15] T.K. Yanai, S. Mori, Density functional studies on thromboxane biosynthesis: mechanism and role of the heme–thiolate system, Chem. Asian. J. 3 (2008) 1900–1911.
[16] T. Matsunobu, T. Okuno, C. Yokoyama, T. Yokomizo, Thromboxane A synthase-independent production of 12-hydroxyheptadecatrienoic acid, a BLT2 ligand, J. Lipid Res. 54 (2013) 2979–2987.
[17] K. Uchida, Current status of acrolein as a lipid peroxidation product, Trends Cardiovasc. Med. 9 (1999) 109–113.
[18] P.C. Dedon, J.P. Plastaras, C.A. Rouzer, L.J. Marnett, Indirect mutagenesis by oxidative DNA damage: formation of the pyrimidopurinone adduct of deoxyguanosine by base propenal, Proc. Natl. Acad. Sci. 95 (1998) 11113–11116.
[19] M.C. Cathcart, J.V. Reynolds, K.J. O'Byrne, G.P. Pidgeon, The role of prostacyclin synthase and thromboxane synthase signaling in the development and progression of cancer, Biochim. Biophys. Acta 1805 (2010) 53–166.
[20] J.E. Abraham, P. Harrington, K.E. Driver, J. Tyrer, D.F. Easton, A.M. Dunning, P.D. Pharoah, Common polymorphisms in the prostaglandin pathway genes and their association with breast cancer susceptibility and survival, Clin. Cancer Res. 15 (2009) 2181–2191.
[21] I.B. Vergote, P.A. van Dam, G.M. Laekeman, G.H. Keersmaeckers, F.L. Uyttenbroeck, A.G. Herman, Prostacyclin/thromboxane ratio in human breast cancer, Tumour Biol. 12 (1991) 261–266.
[22] B.Z. Wang, Y.T. Ma, Z.Y. Fu, X. Xie, X.L. Zhang, B.D. Chen, F. Liu, Z.X. Yu, Association of Rs10487667 genetic polymorphism of thromboxane synthase with myocardial infarction in Uigur population of Xinjiang, Zhonghua Yu Fang Yi Xue Za Zhi 44 (2010) 1032–1036.
[23] Y.V. Grinkova, I.G. Denisov, M.A. McLean, S.G. Sligar, Oxidase uncoupling in heme monooxygenases: human cytochrome P450 CYP3A4 in Nanodiscs, Biochem. Biophys. Res. Commun. 430 (2013) 1223–1227.
[24] I.G. Denisov, S.G. Sligar, Cytochromes P450 in nanodiscs, Biochim. Biophys. Acta 1814 (2011) 223–229.
[25] A. Das, J. Zhao, G.C. Schatz, S.G. Sligar, R.P. Van Duyne, Screening of type I and II drug binding to human cytochrome P450-3A4 in nanodiscs by localized surface plasmon resonance spectroscopy, Anal. Chem. 81 (2009) 3754–3759.
[26] A. Nath, Y.V. Grinkova, S.G. Sligar, W.M. Atkins, Ligand binding to cytochrome P450 3A4 in phospholipid bilayer nanodiscs: the effect of model membranes, J. Biol. Chem. 282 (2007) 28309–28320.
[27] A. Nath, W.M. Atkins, S.G. Sligar, Applications of phospholipid bilayer nanodiscs in the study of membranes and membrane proteins, Biochemistry 46 (2007) 2059–2069.
[28] T. Boldog, S. Grimme, M. Li, S.G. Sligar, G.L. Hazelbauer, Nanodiscs separate chemoreceptor oligomeric states and reveal their signaling properties, Proc. Natl. Acad. Sci. U. S. A. 103 (2006) 11509–11514.
[29] I.G. Denisov, Y.V. Grinkova, A.A. Lazarides, S.G. Sligar, Directed self-assembly of monodisperse phospholipid bilayer Nanodiscs with controlled size, J. Am. Chem. Soc. 126 (2004) 3477–3487.
[30] A. Das, S.S. Varma, C. Mularczyk, D.D. Meling, Functional investigations of thromboxane synthase (CYP5A1) in lipid bilayers of nanodiscs, Chembiochem 15 (2014) 892–899.
[31] Y. Imai, T. Fukuda, M. Komori, M. Nakamura, Comparison of heme environment at the putative distal region of P-450 s utilizing their external and internal nitrogenous ligand bound forms, Biochim. Biophys. Acta Protein Struct. Mol. Enzymol. 1207 (1994) 49–57.
[32] R. Perera, M. Sono, R. Kinloch, H. Zhang, M. Tarasev, S.-C. Im, L. Waskell, J.H. Dawson, Stabilization and spectroscopic characterization of the dioxygen complex of wild-type cytochrome P4502B4 (CYP2B4) and its distal side E301Q, T302A and proximal side F429H mutants at subzero temperatures, Biochimica et Biophysica Acta (BBA)-Proteins and, Proteomics 1814 (2011) 69–75.
[33] A.C. Hasemann, G.R. Kurumbail, S.S. Boddupalli, A.J. Peterson, J. Deisenhofer, Structure and function of cytochromes P450: a comparative analysis of three crystal structures, Curr. Biol. 2 (1995) 41–62.
[34] L.H. Wang, N. Matijevic-Aleksic, P.Y. Hsu, K.H. Ruan, K.K. Wu, R.J. Kulmacz, Identification of thromboxane A2 Synthase active site residues by molecular modeling-guided site-directed mutagenesis, J. Biol. Chem. 271 (1996) 19970–19975.
[35] T. Fukuda, Y. Imai, M. Komori, M. Nakamura, E. Kusunose, M. Kusunose, Replacement of Thr-303 of P450 2E11 with serine modifies the regioselectivity of its fatty acid hydroxylase activity, J. Biochem. 113 (1993) 7–12.
[36] D.R. McDougle, A. Palaria, E. Magnetta, D.D. Meling, A. Das, Functional studies of N-terminally modified CYP2J2 epoxygenase in model lipid bilayers, Protein Sci. 351 (2013) 616–627.
[37] S. Zelasko, A. Palaria, A. Das, Optimizations to achieve high-level expression of cytochrome P450 proteins using *Escherichia coli* expression systems, Protein Expr. Purif. 92 (2013) 77–87.
[38] U. Diczfalusy, P. Falardeau, S. Hammarstrom, Conversion of prostaglandin endoperoxides to C17-hydroxy acids catalyzed by human platelet thromboxane synthase, FEBS Lett. 84 (1977) 271–274.
[39] T.H. Bayburt, Y.V. Grinkova, S.G. Sligar, Self-assembly of discoidal phospholipid bilayer nanoparticles with membrane scaffold proteins, Nano Lett. 2 (2002) 853–856.
[40] B.J. Orlando, D.R. McDougle, M.J. Lucido, E.T. Eng, L.A. Graham, C. Schneider, D.L. Stokes, A. Das, M.G. Malkowski, Cyclooxygenase-2 catalysis and inhibition in lipid bilayer nanodiscs, Arch. Biochem. Biophys. 546 (2014) 33–40.
[41] A. Das, Y.V. Grinkova, S.G. Sligar, Redox potential control by drug binding to cytochrome P450 3A4, J. Am. Chem. Soc. 129 (2007) 13778–13779.
[42] L.A. Kelley, M.J.E. Sternberg, Protein structure prediction on the web: a case study using the Phyre server, Nat. Protoc. 4 (2009) 363–371.